

The role of Metal-Matrix Composite development During Friction Stir Welding of Aluminum to Brass in Weld Characteristics

H.R. Zareie Rajani, A. Esmaili, M. Mohammadi, M. Sharbati, and M.K.B. Givi

(Submitted September 29, 2011; in revised form January 9, 2012)

The present research aims to investigate the development of brass reinforced aluminum composites during dissimilar friction stir welding of brass and aluminum. Moreover, to probe the effect of such a metal matrix composite on its bed, the cross-sectional properties of joint area are studied in two aspects of corrosion behavior and hardness distribution. Microstructural investigations through optical and electron microscopy show development of lamellar composites within the top site of the stir zone and aluminum surface. The measured iso-hardness contours indicate that evolved composite structures increase the cross-sectional hardness of aluminum locally. Also, the electrochemical assessment of joint area suggests that Al/Br composite structure plays an accelerative role in deterioration of cross-sectional corrosion resistance of aluminum through obstructing passivation and forming microgalvanic cells, where cathodic brass reinforcements intensify the corrosion of anodic aluminum matrix.

Keywords aluminum, corrosion testing, metal matrix composites, welding

1. Introduction

Joining of dissimilar materials plays a vital role in vast variety of applications such as military purposes, power generation, and electrical industries. Using conventional joining methods like fusion welding is accompanied by an extreme heat usage, formation of destructive defects, and chemical inhomogeneity, all aggravating the mechanical characteristics and corrosion resistance of weldments (Ref 1). Therefore, friction stir welding (FSW) has been developed as a new solid state welding process to avoid the common welding problems in dissimilar joining, where relative low amount of heat input besides flexibility of procedure can result in better outcomes. FSW process is based on a quite simple concept: A nonconsumable rotating welding tool is plunged into adjoining parent materials. Frictional heat generated by the tool shoulder during this process causes the materials to soften and local plastic deformation to occur. The softened material is stirred together by the rotating tool pin resulting in a solid state bond. The tool design, tool rotation speed, travel speed, tilt angle, depth of

sinking pin, and offset value are dominant parameters in FSW. It should be noted that the offset value refers to the distance of pin from weld interface, featuring in dissimilar FSW.

Several studies carried out about flow of materials in FSW reveal the significant dependency of weld microstructure and consequently weld characteristics upon the material flow (Ref 2, 3). The flow pattern of a stir zone (SZ) arisen from merging of “pin driven” and “shoulder driven” flow might be harsh or as regular as a lamellar pattern called onion rings depending on welding parameters (Ref 3-7). Furthermore, during FSW of dissimilar materials, mixing of distinct material streams in the SZ forms an inhomogeneous composite structure, where distribution of particles through the matrix strongly depends on the shape of flow pattern. Despite the fact that occurrence of such a composite structure alters the characteristics of the SZ, no specific attempt has been made to probe the effect of this local composite structure on the features of a SZ in dissimilar FSW (Ref 8).

Through previous researches (Ref 9, 10), authors have shown the possibility of obtaining a sound joint between brass and aluminum by means of FSW process, where the ultimate tensile strength of the sound joint reaches the 80% that of the base metal, aluminum. In this study, authors aim to investigate the development of local composite structure within the weld-affected zone and consequent effects of that on the properties of its bed, i.e., cross section of weld area. Cross-sectional corrosion resistance and hardness distribution are chosen as two important engineering characteristics to be studied. So far, the majority of investigations into the corrosion behavior of friction stir welded joints are devoted to the similar FSW (Ref 11-15), or the general assessment of dissimilar weld characteristics (Ref 16), regardless of a role played by metal-matrix composites in corrosion properties of dissimilar friction stir welded joints. Undoubtedly, knowing the constructive and/or destructive aspects of this probable influence may contributes to the further ideas about enhancement of weld properties.

H.R. Zareie Rajani, School of Engineering, The University of British Columbia, EME 3223, 3333 University Way, Kelowna, BC V1V 1V7, Canada; A. Esmaili and M.K.B. Givi, School of Mechanical Engineering, University College of Engineering, University of Tehran, Tehran, Iran; M. Mohammadi, School of Materials Science and Engineering, Sharif University of Technology, Tehran, Iran; and M. Sharbati, School of Materials Science and Engineering, University College of Engineering, University of Tehran, Tehran, Iran. Contact e-mail: hamid.r.zareie@ut.ac.ir.

2. Material and Methods

Three millimeters thickness Brass and aluminum 1050H16 sheets with chemical compositions given in Table 1 and 2 were used to fabricate FSW butt joints. The 140 × 80 mm plates were fixed in butt position by a fixture during welding. Also, the tool was made of hot working alloy steel (1.2344) which its hardness reached 45HRC after heat treatment. Furthermore, as Fig. 1 depicts the geometry of used tool, the tool was composed of a 15 mm diameter shoulder and a tapered slotted pin. According to the former study on FSW of brass and aluminum, the pin location was shifted towards aluminum as a softer material, and welding parameters listed in Table 3 were applied to reach an optimum defect free joint (Ref 9). Also, the aluminum was selected as retreating side whereas brass played the role of advancing side, where the tool forged aluminum to brass.

Optical microscopy and scanning electron microscopy were utilized to investigate the microstructural characteristics of weld. In addition, the Vickers microhardness measurement was carried out along the seven parallel lines laying on the cross

section of joint using 100 g load and 10 s for every measurement. Part of indentations is depicted in Fig. 2. Although the line spacing decreased by approaching the top surface of sample to enhance the hardness measurements through composite structure, a minimum line spacing was applied to avoid interference of indentations. Then, in order to probe the hardness variation, the measured hardnesses were implemented to plot the cross-sectional iso-hardness contours.

The electrochemical method was applied to assess the corrosion behavior of aluminum as bed of composites. First, the cross section of weld was polished after a sequential grinding to

Table 1 Chemical composition of aluminum 1050

Material	Al	Ti	Zn	Mn	Fe	Si	Mg	Cu
Al1050	Balance	0.05	0.07	0.05	0.4	0.25	0.05	0.05

Table 2 Chemical composition of brass

Material	Sn	Pb	P	Mn	Fe	Ni	Si	Mg	Al	Zn	Cu
CuZn30	0.1	0.005	...	0.05	0.05	0.3	0.25	0.05	0.02	Balance	69

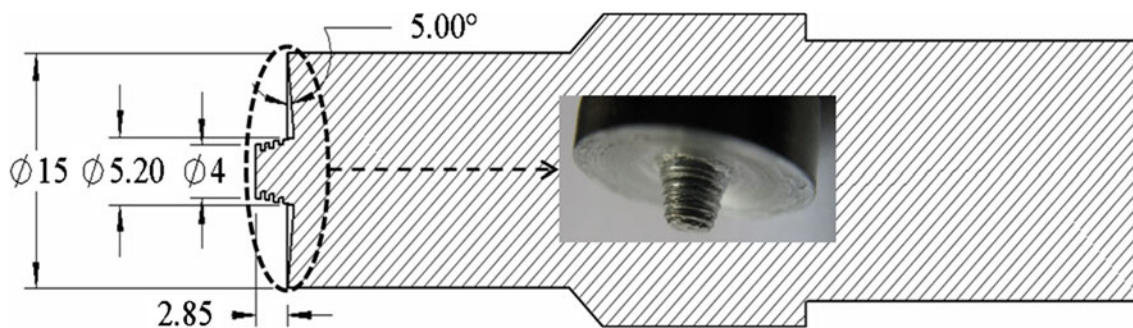


Fig. 1 The schematic view of used tool showing geometry and dimensions

Table 3 The optimum welding parameters applied to produce sound joint

Welding parameter	Rotation speed, rpm	Travel speed, mm/min	Offset value, mm	Tilt angle, °	Depth of sinking pin, mm
Value	450	8	+1.6	1.5	0.25

Note that positive sign of offset value corresponds to shifting of tool towards aluminum

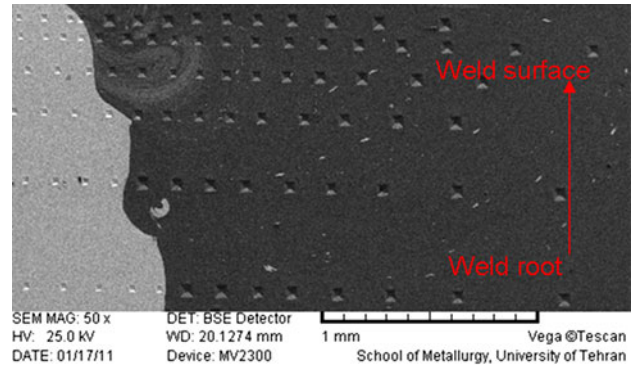


Fig. 2 Part of Vickers microhardness indentations applied to plot cross-sectional iso-hardness contours

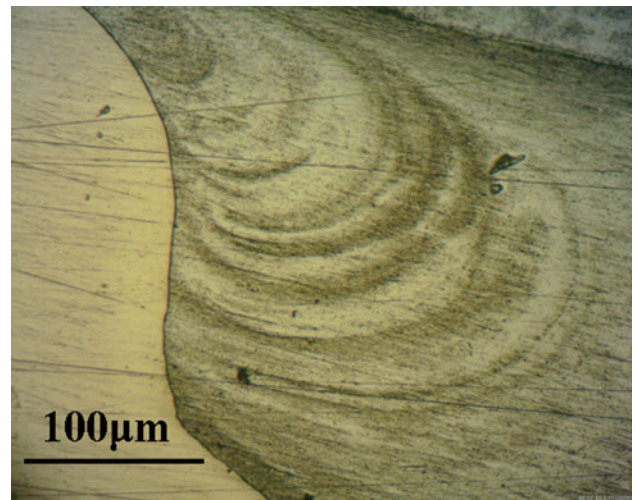
eliminate the surface contaminants and scratches. Also nail polishing was applied to cover the unwanted regions and expose the selected desired cross-sectional zones to corrosive environment. Then the potentiodynamic polarization was carried out in a 3.5 wt.% NaCl solution at ambient temperature regarding the ASTM G5 standard (Ref 17). The Platinum and Ag/AgCl electrodes were chosen as counter and reference, respectively. Also, it is important to note that the scanning rate of 1 mv/s was applied to polarize the desired area of surface. Finally, the corrosion rate (i_c) measured by Tafel extrapolation technique and protection current density (i_p) were studied as main corrosion characteristic of aluminum.

3. Results and Discussion

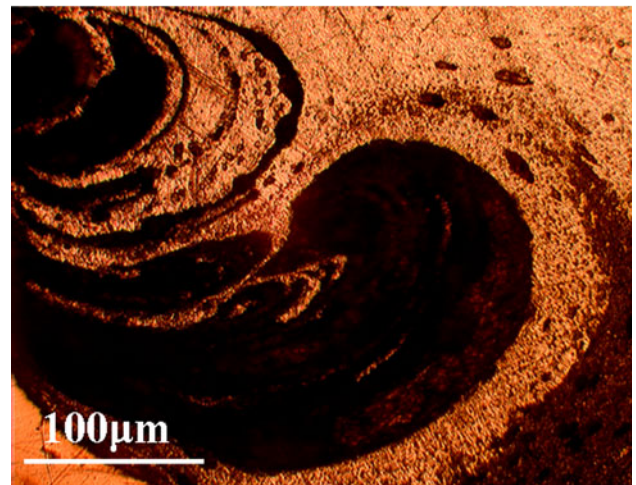
3.1 Microstructure

As Fig. 3 shows, the cross section of aluminum side can be divided into two main distinguished areas after welding: (i) the weld-affected area including the SZ located within aluminum, shoulder affected zone (SAZ) evolving at the weld surface and thermo-mechanical affected zone (TMAZ) in vicinity of SZ. (ii) The unaffected area placed far away from the weld interface.

Figures 3 and 4 reveal the existence of onion rings as an obvious feature of the SZ. This lamellar flow pattern is attributed to the noncontinuous extrusion of aluminum through FSW (Ref 5). Such an extrusion occurs due to coincidence of aluminum plasticization arisen from frictional heating and stirring of pin. Also, since a short-time interval is needed to generate sufficient amount of frictional heat prior to each extrusion, this phenomenon occurs periodically rather than continuously. Though even a just polished surface reveals the existence of onion rings (Fig. 4a), etching the samples highlights rings (Fig. 4b) due to preferential attack of etchant on onion rings. Furthermore, backscattered electron images of the SZ show the existence of a local composite structure consisting of fine brass particles scattered as reinforcing components through aluminum matrix (Fig. 5a, b). Evolution of such a composite structure during dissimilar FSW of brass and



(a)



(b)

Fig. 4 Onion rings within the SZ, indicating the lamellar flow of material. (a) Just polished surface and (b) etched surface

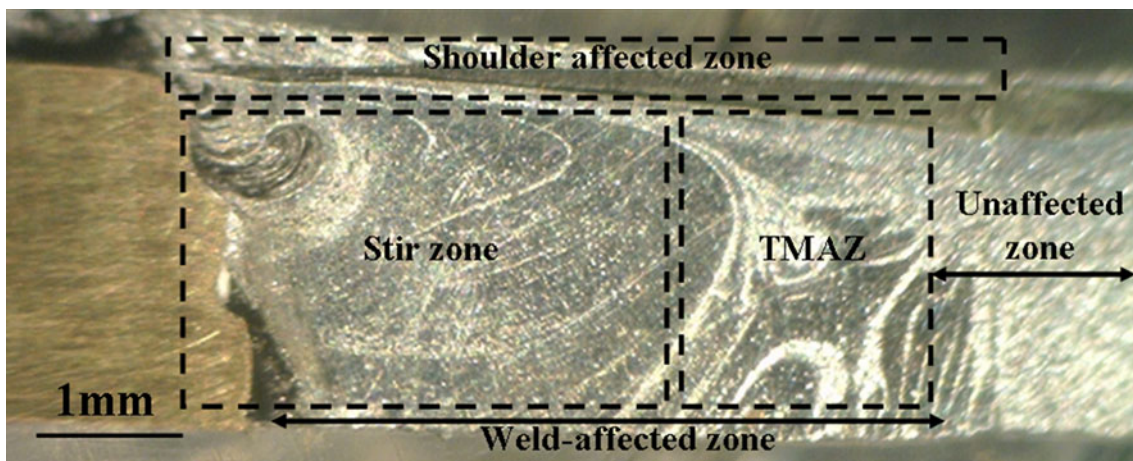


Fig. 3 Division of aluminum cross section into two main areas after welding: weld-affected zone and unaffected zone

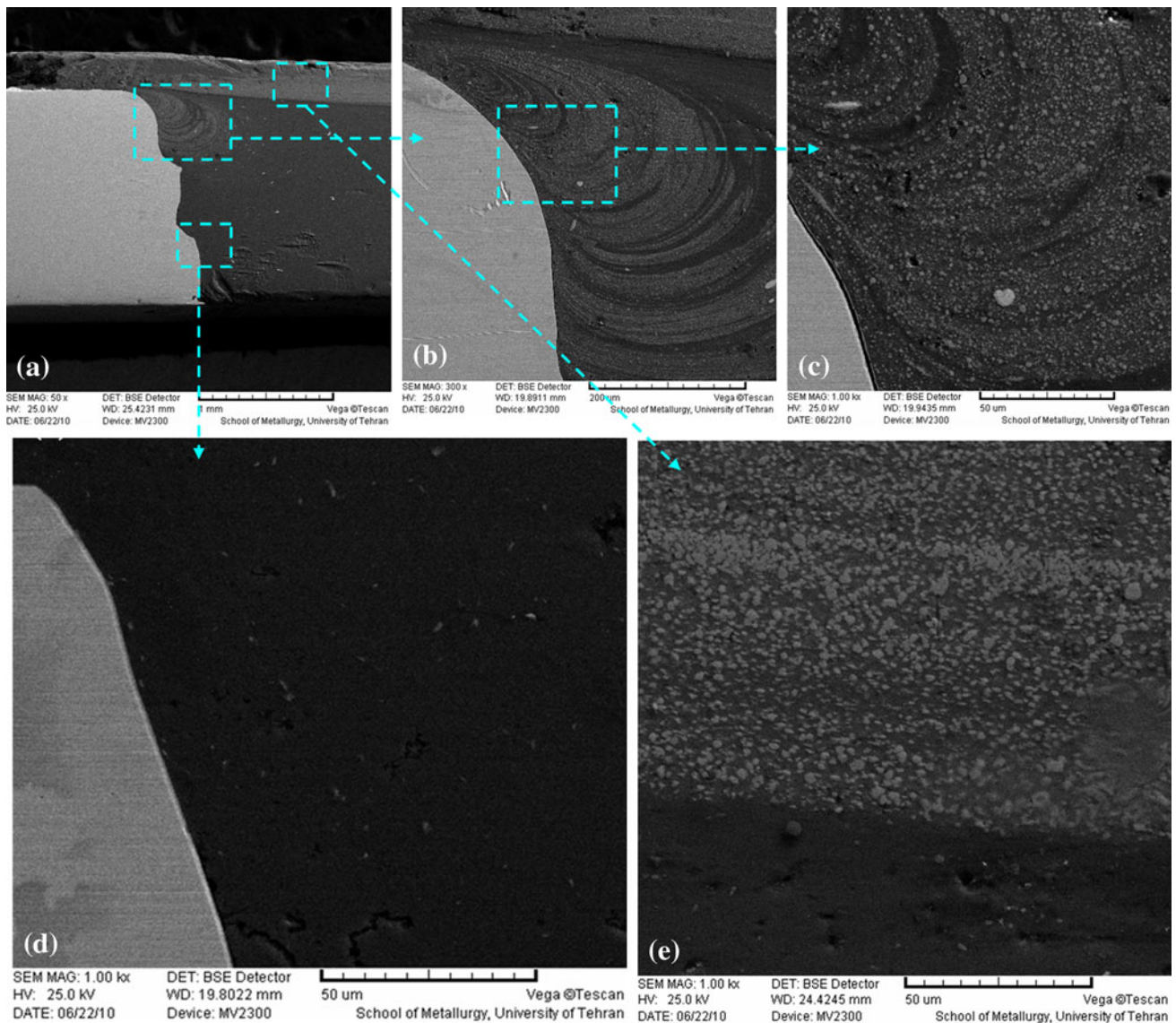


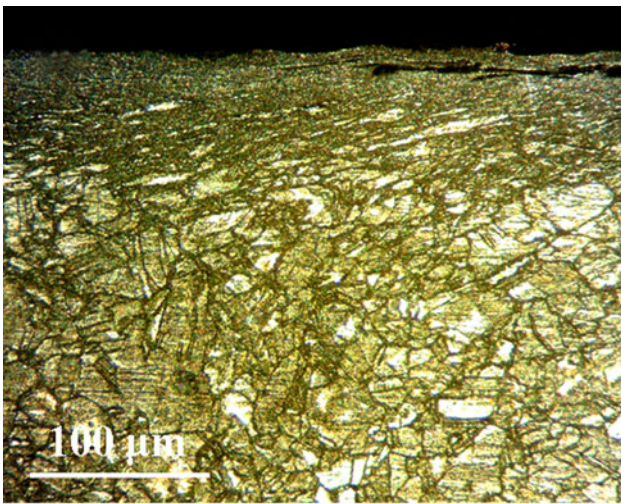
Fig. 5 (a) Backscattered electron image of weld cross section after welding, (b) the lamellar Al/Br composite structure within top of the SZ, (c) close view of lamellar composite structure, (d) bottom area of the SZ, and (e) the Al/Br composite structure evolved on aluminum surface in SAZ

aluminum can be ascribed to simultaneous plasticization of brass besides forces imposed by aluminum extrusion on the weld interface, all facilitating the interfacial crumbling of brass through periodic extrusion. As Fig. 5(b) and (c) depicts the lamellar distribution of brass particles in this local composite structure, accumulation of particles within onion rings endorses the role of periodic extrusion in brass fragmentation and development of composite structure within the SZ. Also, due to lack of brass plasticization in lower areas, mainly issuing from heat shortage, the composite structure vanishes near bottom of the SZ (Fig. 5d). Note that such fine particles are observed just in optimum welding condition, and excessive or insufficient frictional heat and extrusion force may end in appearance of coarse brass fragments or complete disappearance of composite structure (Ref 9).

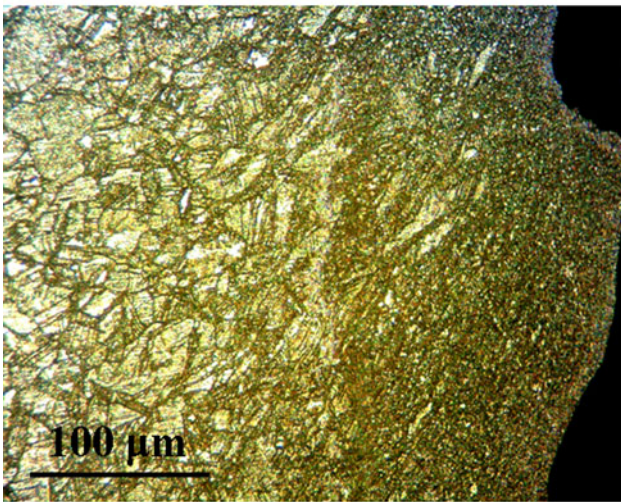
Close observation of SAZ by backscattered electron images suggests the occurrence of a surface composite structure on

aluminum surface, where shoulder crumbles the surface layer of brass over aluminum matrix as retreating side (Fig. 5a, e). So, in addition to a composite structure evolved in the SZ, a similar structure develops at the surface of aluminum side. Note that in contrast with SZ and SAZ, the TMAZ does not contain any composite structure.

After detecting local composite structure in various observed sites of the weld including SZ and SAZ, it is important to probe the impact of severe plastic deformation on the weld microstructure. Figure 6(a) and (b) shows a grain size gradient observed through the brass side, where by increment of plastic strain in vicinity of interface and weld surface the grain size declines. This severe strain-induced grain refinement can be attributed to the crystal structure of brass possessing low stacking fault energy (0.01 J/m^2), the fact that promotes the mechanical twinning and development of strain-induced subgrains besides obstructing dynamic recovery (Ref 18, 19). On



(a)



(b)

Fig. 6 Grain size gradient through brass side. (a) In vicinity of top surface and (b) near the weld interface

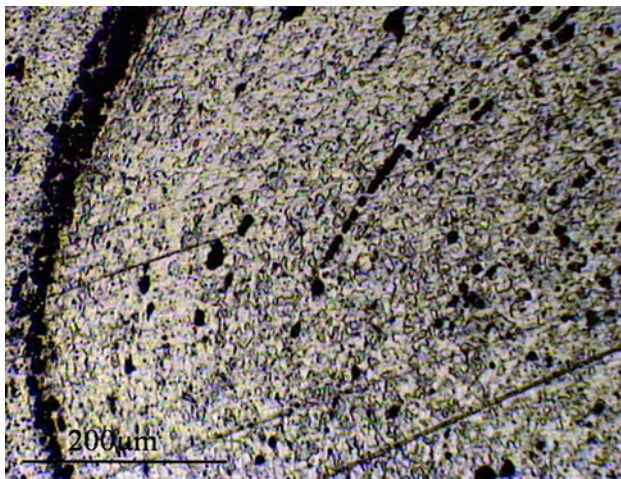


Fig. 7 Uniform size of grains through aluminum side after welding

the other hand, obtained results reveal that severe plastic deformation can not create such a sharp grain size gradient in aluminum side where grains possess quite uniform size (Fig. 7). As a matter of fact, aluminum with its very high stacking fault energy, about 0.16 J/m^2 , shows extensive dynamic recovery and thus lower strain hardening than does brass during FSW.

3.2 Hardness Distribution

Figure 8 depicts the cross-sectional iso-hardness contours of the weld area. As it is seen, the hardness distribution over the weld zone does not show a uniform trend. The aluminum hardness increases obviously in top of the SZ and the weld surface where the local composite structures occur. Figure 9(a) showing the optical image of Vickers indentations, highlights the decrement of indentation size by entering top of the SZ. The observed decrease in penetration ability of indenter through these mentioned regions can be mainly ascribed to the existence of local brass reinforced aluminum composite structures (Fig. 9b). Fine brass particles scattered within the local composite structure reinforce the aluminum matrix, leading to more resistance against penetration of indenter into the aluminum.

Moreover, the brass hardness shows a significant increase in vicinity of the weld interface and the weld surface. This phenomenon issues from strain-induced grain refinement besides strain hardening effect occurring in these regions (Fig. 6a, b). As a result, despite the fact that dynamic recovery of aluminum obstructs the increment of aluminum hardness through strain hardening, the evolution of local composite structures escalates the aluminum hardness locally.

3.3 Corrosion Behavior

Regarding the fact that developed composites are sited within aluminum side, the corrosion resistance of aluminum is probed to understand the effect of composite structures on corrosion behavior of weld area. Aluminum is highly reactive metal possessing a high resistance to corrosion attack in many environments due to the presence of a thin adherent film of aluminum oxide. Despite the fact that this oxide film improves the corrosion resistance of aluminum, formation of a defective or damaged protective layer makes aluminum prone to localized corrosion (Ref 20). High amount of alloying elements, chemical inhomogeneity, or structural nonuniformity are the major factors disturbing uniform development of a perfect adherent oxide film on aluminum surface. Moreover, mechanical or chemical surface damages can also contribute to localized corrosion (Ref 21).

Figure 10 illustrates the position of two distinct cross-sectional areas of aluminum which their corrosion behavior is assessed separately by potentiodynamic polarization. The Zone A contains the weld-affected region, whereas the Zone B is selected far away from weld interface to measure the corrosion behavior of unaffected area in aluminum. The potentiodynamic polarization outcomes are shown in Fig. 11. Furthermore, the corrosion rates extracted by Tafel extrapolation technique besides passivation current densities are listed in Table 4. Comparison of electrochemical corrosion characteristics in various studied cross-sectional zones suggests the detrimental effect of FSW on corrosion resistance of aluminum, where the

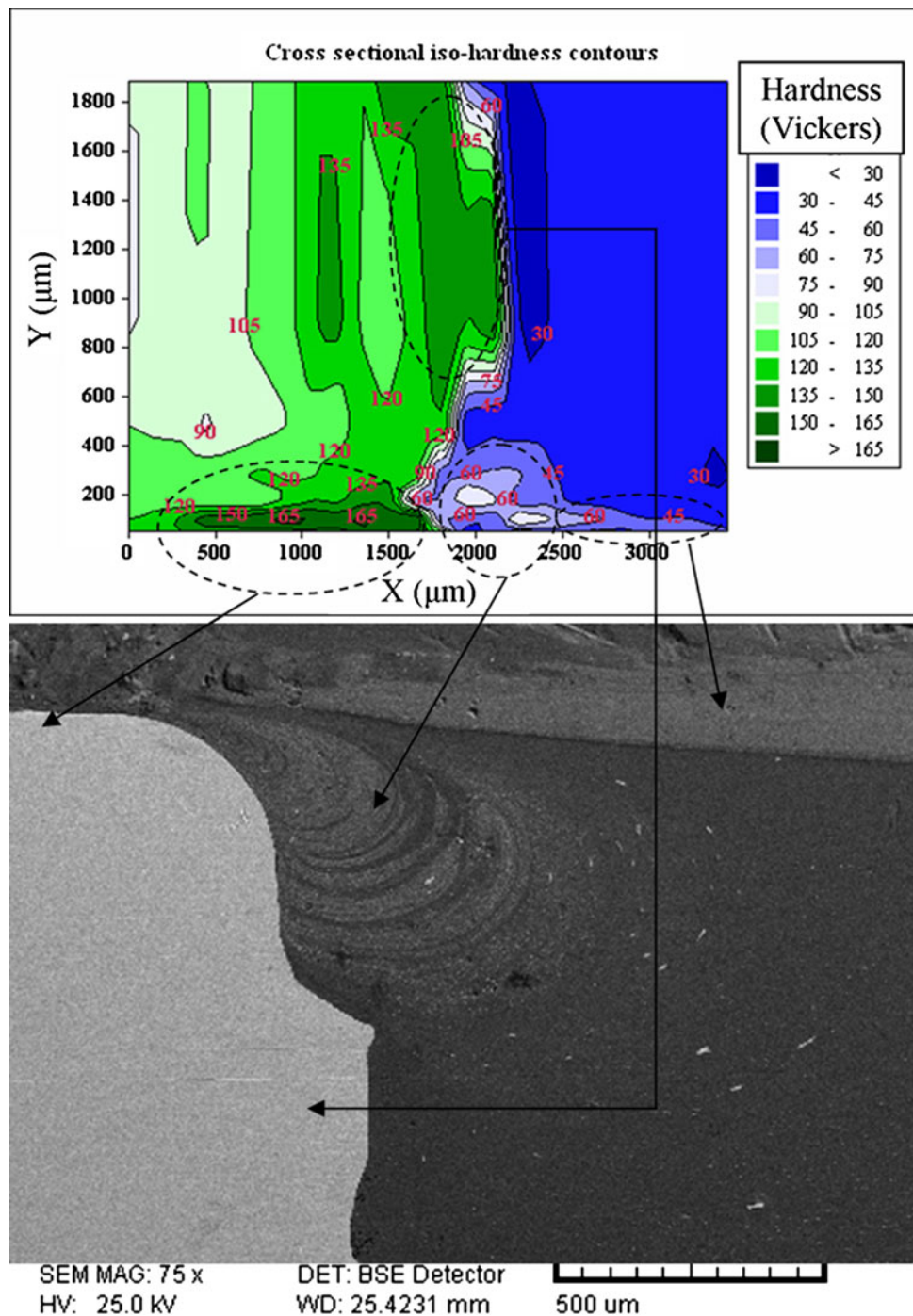


Fig. 8 Cross-sectional iso-hardness contours corresponding to hardness measurements shown in Fig. 2

corrosion rate escalates significantly in the weld-affected zone, i.e., Zone A (Table 4). Since the welds are not usually used as an isolated part in mechanical designs, and they are in contact with other materials, they might act as anodic component in a corrosion system. As a result, studying the anodic behavior of welds besides the corrosion rate can reveal the quality of corrosion resistance more efficiently. As Fig. 11 indicates, Zone A does not show a sharp and clear passivation behavior relative to the unaffected area (Zone B) where a sudden intense

increment in slope of anodic branch represents the formation of passive layer on aluminum surface. In order to interpret the observed differences, the variation of anodic current density versus time of polarization has been plotted in Fig. 12. As variation of anodic current density with respect to time in region B suggests (Fig. 12a), the surface passivation leads to a mild corrosion situation where the anodic current density under an approximate linear behavior cannot exceed the value of 0.1 A/Cm^2 in the applied range of polarization. On the other

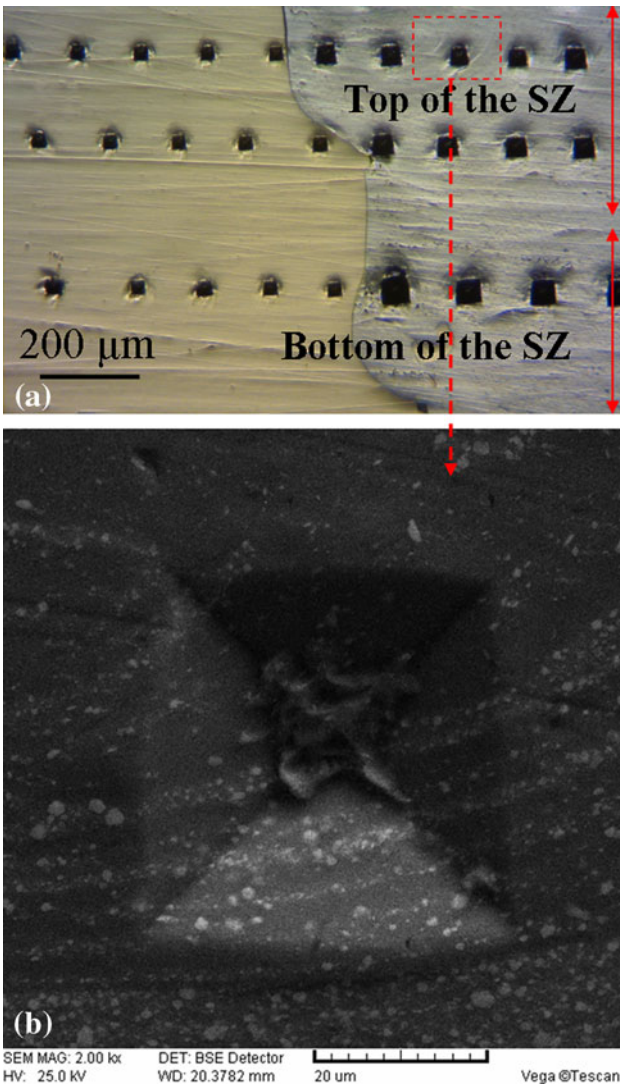


Fig. 9 (a) Decrement of Vickers indentation size by approaching top of the SZ and (b) close observation of Vickers indentation within top of the SZ

hand, studying the variation of anodic current density in Region A reveals a harsh corrosion situation where the current density changes exponentially in the applied range of polarization, and does not show any intend towards retarding the corrosion attack (Fig. 12b). So, as Fig. 12(a) and (b) illustrates, if present weld be exposed to a cathodic couple which brings the weld to a specific anodic overvoltage after a specific time (t_0), the Zone A will be much more vulnerable to corrosion attack, unlike the unaffected area (Zone B) which can resist the attack satisfactorily. Figure 10 depicting the aluminum surface after potentiodynamic polarization justifies the observed electrochemical corrosion behavior variation through aluminum side, where the weld-affected area undergoes severe localized corrosion but unaffected zone does not show any sign of severe corrosion attack.

Such a variation in cross-sectional corrosion behavior of aluminum side can be attributed to two main factors. First of all, evolution of an imperfect aluminum oxide film over the

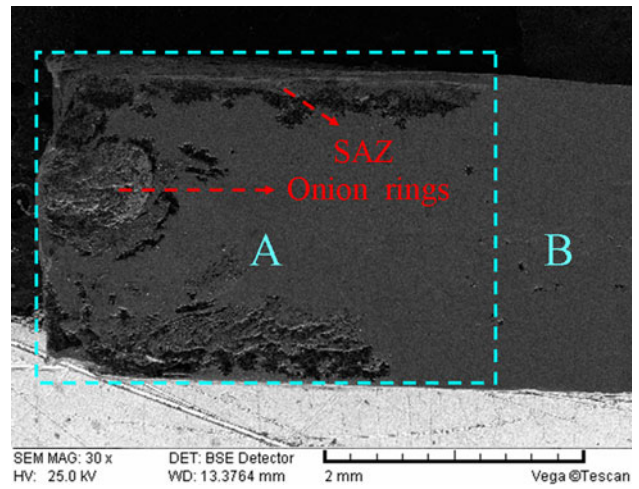


Fig. 10 Various cross-sectional regions of aluminum selected to study their corrosion behavior. Image shows aluminum cross section after carrying out corrosion tests. Zone A includes the weld-affected zone and Zone B is unaffected area

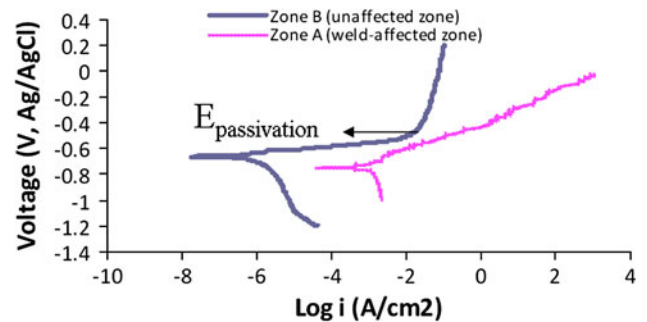


Fig. 11 Potentiodynamic polarization diagrams of the weld-affected zone and unaffected area of aluminum cross section. Zones A and B correspond to weld-affected and unaffected regions respectively, as shown in Fig. 10

Table 4 The corrosion characteristics of weld-affected zone and unaffected region in aluminum cross section

Zones	Corrosion rate, mA/Cm ²	Passivation current density, mA/Cm ²
A (weld-affected zone)	1.26	...
B (unaffected zone)	0.0019	25

Zones A and B are shown in Fig. 10

weld-affected zone, the fact which tallies with obscure passivation behavior of Zone A recorded through polarization diagrams (Fig. 11; Table 4). Regarding the fact that solid state welding cannot alter the chemical composition, it is deduced that such an impediment to evolution of protective film may emanates from structural nonuniformity of aluminum occurring through FSW. This nonuniformity comes from two major

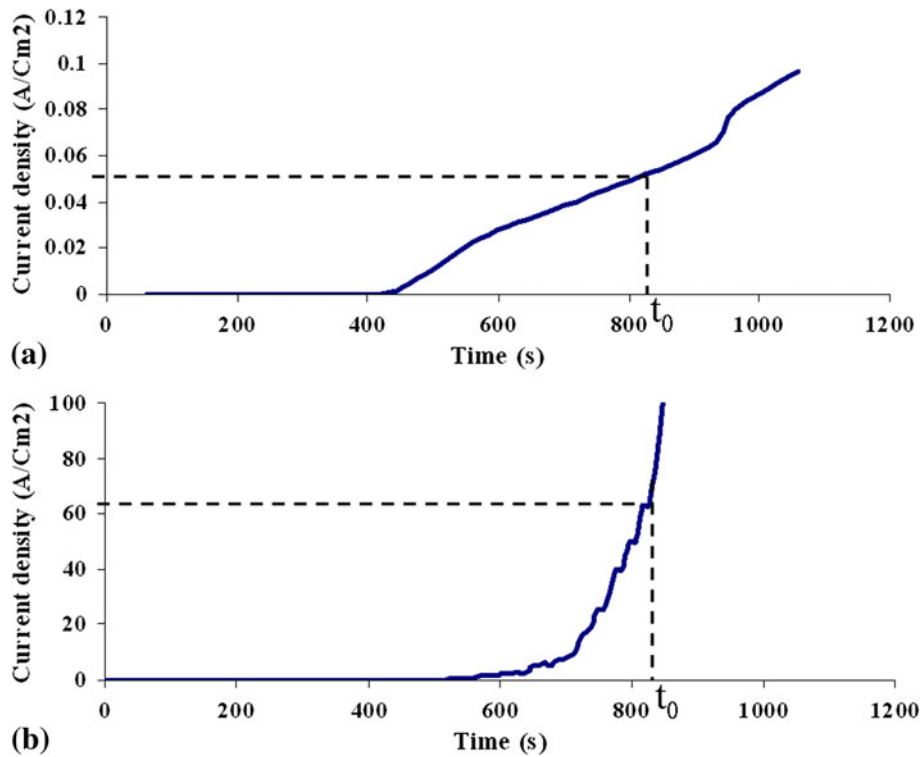


Fig. 12 The variation of current density versus time of polarization; (a) unaffected area (Zone B), (b) weld-affected area (Zone A)

sources: structural defects and brass particles scattered through composite structures. Structural defects like vacancies and dislocations developed during FSW lead to evolution of a defective protective film which makes the weld-affected zone vulnerable to corrosion attack (Ref 20). Also, existence of brass particles within local composite structures disturbs the chemical homogeneity of aluminum surface being vital for development of a perfect protective film over aluminum surface (Ref 21).

The second factor which aggravates corrosion behavior in the weld-affected zone can be corrosion amplification due to residual strains and microgalvanic cells occurring through composite structures. The residual strain of weld-affected zone intensifies corrosion attack by increasing the free energy density (Ref 22). Moreover, as it is reported through various studies (Ref 23, 24), due to direct contact of dissimilar materials, the microgalvanic corrosion can play an accelerative role in corrosion of composite structures. Since brass possesses a higher standard reduction potential relative to aluminum (Ref 20), a microgalvanic cell may form within observed composite structures, where brass particles as cathodic reinforcements accelerate the corrosion of aluminum as anodic matrix. Concentration of corrosion attack on areas with higher brass particles density like onion rings within the SZ confirms the role of microgalvanic cells in corrosion of aluminum (Fig. 13a). Moreover, as Fig. 13(b) illustrates, brass particle does not undergo a severe attack, unlike adjacent aluminum matrix experiencing a severe corrosion, the fact which verifies the

cathodic role of brass and anodic role of aluminum within a local brass reinforced aluminum composite structure.

On the other hand, a perfect adherent film covering the unaffected area obstructs the severe corrosion attack. Consequently, the higher corrosion rates measured in the weld-affected zone can be ascribed to a weaker protection mechanism in this area relative to the unaffected zone in addition to acceleration of corrosion. The phenomena arisen from simultaneous detrimental effect of structural defects, residual strain, and existence of local brass reinforced aluminum composites.

4. Conclusions

According to the obtained results, local brass reinforced aluminum composites evolve within top site of the SZ and aluminum surface through dissimilar FSW of brass and aluminum. These lamellar composite structures increase the cross-sectional hardness of aluminum locally due to reinforcing role of fine brass particles scattered within aluminum matrix.

In addition, results reveal the detrimental role of FSW on cross-sectional corrosion behavior of aluminum side, where existence of brass particles within composite structures besides the structural nonuniformity aggravates the passivation ability of the weld-affected zone, and residual strains in addition to microgalvanic cells occurring in local composites heighten the corrosion rate of this region.

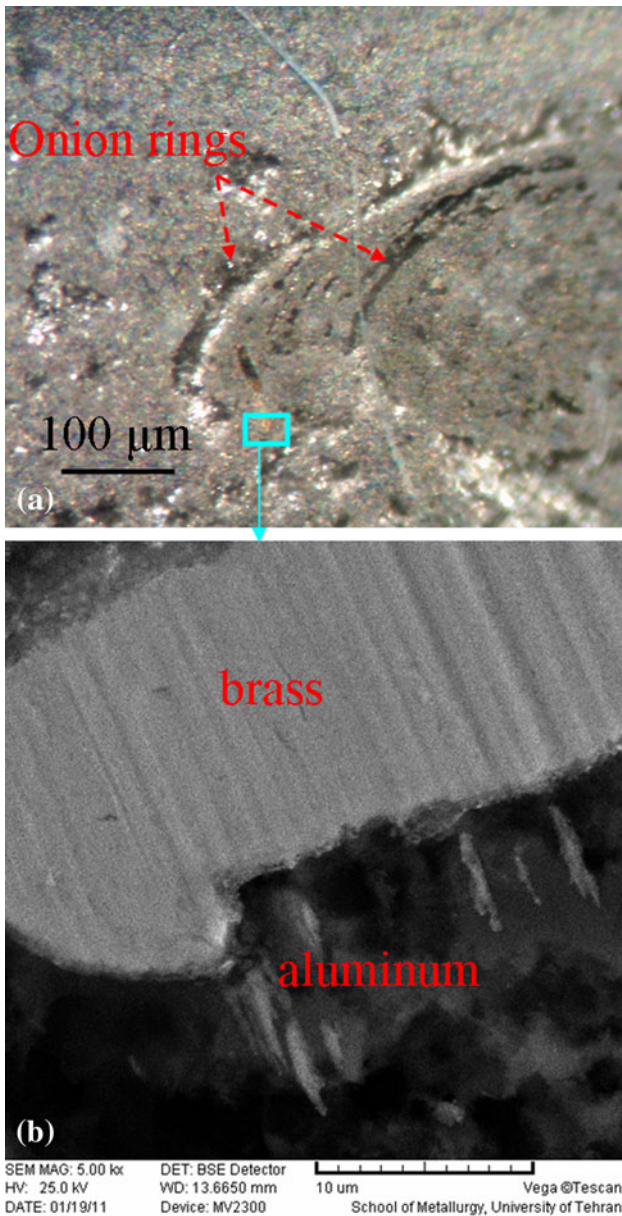


Fig. 13 (a) Preferential corrosion attack on onion rings containing brass particles and (b) close view of brass particle and adjacent aluminum matrix after corrosion

References

- M.D. Fuller, S. Swaminathan, A.P. Zhilayev, and T.R. McNelley, Microstructural Transformations and Mechanical Properties of Cast NiAl Bronze: Effects of Fusion Welding and Friction Stir Processing, *Mater. Sci. Eng. A*, 2007, **463**, p 128–137
- H.N.B. Schmidt, T.L. Dickerson, and J.H. Hattel, Material Flow in Butt Friction Stir Welds in AA2024-T3, *Acta Mater.*, 2006, **54**, p 1199–1209
- Z.W. Chen, T. Pasang, and Y. Qi, Shear Flow and Formation of Nugget Zone During Friction Stir Welding of Aluminum Alloy 5083-O, *Mater. Sci. Eng. A*, 2008, **474**, p 312–316
- Y. Yan, D. Zhang, C. Qiu, and W. Zhang, Dissimilar Friction Stir Welding Between 5052 Aluminum Alloy and AZ31 Magnesium Alloy, *Trans. Nonferrous Met. Soc.*, 2010, **20**, p s619–s623
- K.N. Krishnan, On the Formation of Onion Rings in Friction Stir Welds, *Mater. Sci. Eng. A*, 2002, **327**, p 246–251
- A.A.M. da Silva, E. Arruti, G. Janeiro, E. Aldanondo, P. Alvarez, and A. Echeverria, Material Flow and Mechanical Behaviour of Dissimilar AA2024-T3 and AA7075-T6 Aluminium Alloys Friction Stir Welds, *Mater. Des.*, 2011, **32**, p 2021–2027
- K. Kumar and S. Kailas, The Role of Friction Stir Welding Tool on Material Flow and Weld Formation, *Mater. Sci. Eng. A*, 2008, **485**, p 367–374
- R.S. Mishra and Z.Y. Ma, Friction Stir Welding and Processing, *Mater. Sci. Eng. R*, 2005, **50**, p 1–78
- A. Esmacili, M.K. Besharati Givi, and H.R. Zareie Rajani, A Metallurgical and Mechanical Study on Dissimilar Friction Stir Welding of Aluminum 1050 to Brass (CuZn30), *Mater. Sci. Eng. A*, 2011, **528**, p 7093–7102
- A. Esmacili, H.R. Zareie Rajani, M. Sharbati, M.K. Besharati Givi, and M. Shamanian, The Role of Rotation Speed on Intermetallic Compounds Formation and Mechanical Behavior of Friction Stir Welded Brass/Aluminum 1050 Couple, *J. Intermet.*, 2011, **19**, p 1711–1719
- M. Jariyaboon, A.J. Davenport, R. Ambat, B.J. Connolly, S.W. Williams, and D.A. Price, The Effect of Welding Parameters on the Corrosion Behaviour of Friction Stir Welded AA2024-T351, *Corros. Sci.*, 2007, **49**, p 877–909
- C.S. Paglia and R.G. Buchheit, A Look in the Corrosion of Aluminum Alloy Friction Stir Welds, *Scripta Mater.*, 2008, **58**, p 383–387
- R.W. Fonda, P.S. Pao, H.N. Jones, C.R. Feng, B.J. Connolly, and A.J. Davenport, Microstructure, Mechanical Properties, and Corrosion of Friction Stir Welded Al 5456, *Mater. Sci. Eng. A*, 2009, **519**, p 1–8
- J. Kang, R. Fu, G. Luan, C. Dong, and M. He, In-Situ Investigation on the Pitting Corrosion Behavior of Friction Stir Welded Joint of AA2024-T3 Aluminium Alloy, *Corros. Sci.*, 2010, **52**, p 620–626
- D.A. Wadson, X. Zhou, G.E. Thompson, P. Skeldon, L. Djapic Oosterkamp, and G. Scamans, Corrosion Behaviour of Friction Stir Welded AA7108 T79 Aluminium Alloy, *Corros. Sci.*, 2006, **48**, p 887–897
- C. Liu, D.L. Chen, S. Bhole, X. Cao, and M. Jahazi, Polishing-Assisted Galvanic Corrosion in the Dissimilar Friction Stir Welded Joint of AZ31 Magnesium Alloy to 2024 Aluminum Alloy, *Mater. Charact.*, 2009, **60**, p 370–376
- Standard ASTM G5 1994
- G.E. Dieter, *Mechanical Metallurgy*, 3rd ed., McGraw-Hill, Boston, 1986
- J. Cai, S. Shekhar, J. Wang, and M. Ravi Shankar, Nanotwinned Microstructures from Low SFE Brass by HRSPD, *Scripta Mater.*, 2009, **60**, p 599–602
- M.G. Fontana, *Corrosion Engineering*, 3rd ed., McGraw-Hill, New York, 1986
- R. Baboian, *Corrosion Tests and Standards, Application and Interpretation*, 2nd ed., ASTM International, West Conshohocken, 2005
- D. Lewis, D.O. Northwood, and C.E. Pearce, A Study of the Effects of Microstrain on the Electrode Potential and the Anodic Dissolution of Cu, *Corros. Sci.*, 1969, **9**, p 779–787
- S. Tiwari, R. Balasubramaniam, and M. Gupta, Corrosion Behavior of SiC Reinforced Magnesium Composites, *Corros. Sci.*, 2007, **49**, p 711–725
- N.N. Aung, W. Zhou, C.S. Goh, S.M.L. Nai, and J. Wei, Effect of Carbon Nanotubes on Corrosion of Mg-CNT Composites, *Corros. Sci.*, 2010, **52**, p 1551–1553